A Simple and Effective Predictive Power Control for Induction Motor Drives

Jin Zhang, *Student Member, IEEE*, Zhenbin Zhang, *Senior Member, IEEE*, Zhen Li, *Member, IEEE*, Haitao Li, *Student Member, IEEE*, Yongdu Wang, *Student Member, IEEE*, Shichang Zhou, *Student Member, IEEE*, and Teng Long, *Member, IEEE*

***Abstract*—Predictive current control techniques rely on the accuracy of flux angle detection, which seriously impacts the control performances for induction motor drives. Aiming at this, many researches have been proposed to improve the flux angle detection accuracy, which usually complicates the system design and algorithm realization. In this work, we propose an effective and simple *predictive power control* strategy for induction motors that omits flux angle detection and simplifies the system design. Similar to classical predictive torque control, the proposal does not require flux angle information. Moreover, it requires no weighting factor design process. In addition, a stable flux observer in the stationary coordinate system is proposed and the conditions to satisfy Lyapunov stability are detailed. The effectiveness of this work is verified by experimental data. Compared with the classic predictive control strategies, the proposed method shows superior steady and dynamic performances with a simplified control structure and realization.**

***Index Terms*—Induction motor, instantaneous power, predictive power control (PPC), simplified control framework.**

I. Introduction

MODEL predictive control (MPC) is a simple and fast-developing technique that has very fast control dynamic and flexible multiobjective capability, and now has become a promising technique for power electronics, motor drives, renewable energy systems, etc. [1], [2], [3], [4]. Predictive current control (PCC) is one of the most classical predictive control sub-classes for induction motor (IM) drives. However, precise flux angle detection is key to achieving great control performance for PCC. It is also a big challenge for this strategy to obtain excellent control performance. Generally, there are two classical methods for flux angle detection, i.e., speed integral and phase-locked loop (PLL). The former is the integral of the sum of slip speed and electrical angular speed. The accuracy of this method highly relies on the identification of rotor time constant (T_r) which is essential to obtain slip speed [5]. Compared with the rotor inductance (L_r) which can be updated online by a preset magnetizing curve [6], the rotor resistance (R_r) is more difficult to obtain. R_r is highly coupled with the temperature, which is easy to fluctuate and difficult to analyze with the changes of load and working time. Hence T_r will also fluctuate with R_r, which will lead to the deviation of flux angle detection. This mismatch will seriously affect the performance of the IM drives.

To solve this problem, online T_r identification is an effective solution, which includes spectral analysis, observer-based method, model reference adaptive system (MRAS), and artificial intelligence (AI) methods [7], [8]. The spectral analysis method is to obtain T_r by analyzing the characteristics of the injected signal response [9] or specific harmonics in the current or voltage spectrum [10]. The observer-based method mainly includes extended Kalman filter (EKF) [11], Luenberger observer, and sliding mode observer (SMO) [12]. Among them, a R_r and L_r estimation methodology based on EKF without no-load or locked-rotor tests was proposed in [11]. A Luenberger-SMO was proposed in [12], which has faster tracking of parameter changes and improved robustness, and it is consistent with the classical Luenberger observer when the parameter changes are small. MRAS is an effective method in the field of parameter estimation, because of its simple structure and easy implementation. Therefore, there are many T_r estimation methods using MRAS, such as rotor flux [13], stator voltage [14], torque [15], or reactive power [16]. With the increase of controller computing power, AI has also become a promising online T_r estimation method. For example, artificial neural networks were used in [17] to compute the parameters during transients. The authors in [18] proposed an adjustable particle swarm optimization algorithm to update the variation of T_r. Scholars have proposed many effective solutions to the time-varying T_r, but they usually increase the complexity of implementation. In addition, the control performances are also

Manuscript received 4 December 2023; revised 2 April 2024; accepted 13 May 2024. Date of publication 5 June 2024; date of current version 11 September 2024. This work was supported in part by the National Key R&D Program of China under Grant 2022YFB4201700, in part by the General Program of National Natural Science Foundation of China under Grant 51977124, Grant 52277191, and Grant 52277192, in part by the Shenzhen Fundamental Research Program under Grant JCYJ20210324132616040, and in part by Jinan "Several Policies on Promoting Collaborative Innovation and Achievement Industrialization of Universities and Research Institutes (Trial)" under Grant 2020GXRC009. Recommended for publication by Associate Editor L. V. Iyer. *(Corresponding author: Zhenbin Zhang.)*

Jin Zhang, Zhenbin Zhang, Zhen Li, Haitao Li, and Shichang Zhou are with the School of Electrical Engineering, Shandong University, Jinan 250100, China (e-mail: zbz@sdu.edu.cn).

Yongdu Wang is with the Chair of High-Power Converter Systems, Technical University of Munich, 80333 Munich, Germany.

Teng Long is with the Electrical Engineering Division, Department of Engineering, University of Cambridge, CB2 1TN Cambridge, U.K..

Color versions of one or more figures in this article are available at https://doi.org/10.1109/TPEL.2024.3404069.

Digital Object Identifier 10.1109/TPEL.2024.3404069

affected by the depth of the detail and the available resources during the implementation [8].

Compared with speed integral, the PLL schemes are more robust to L_{r} variation. However, there is a phase error when the speed ramps because the classical PLL is a type-2 control system [19]. Increasing the control bandwidth can effectively reduce this phase error, but its disturbance rejection capability will be reduced. To solve this problem, the authors in [20] proposed adaptive PLL that increases the control bandwidth to reduce phase error and improve the dynamic response when the speed ramps, and decreases the bandwidth in the steady state to keep disturbance rejection capability. To maintain the phase without deviation, some scholars propose high-order PLL or variable structure PLL [21]. In addition, the performances of PLL can be affected by the harmonics and dc bias [22]. To improve the disturbance rejection capability of PLL, many scholars incorporate specially designed filters in front of the input or inside the control loop of PLL. The authors in [23] proposed a scheme to improve the disturbance suppression capability of PLL by adding a moving average filter that can completely block the specific frequency disturbance. However, adding an additional filter causes the transient performance to deteriorate, and the PI controller in the loop filter is replaced by the PID controller. According to different application backgrounds, some scholars have proposed to use notch filter, complex coefficient filter, and second-order generalized integrator to improve the disturbance rejection capability of PLL [24]. As far as the dc bias problem, adding a bias suppression ring inside the PLL is an effective method to solve it. The input of the PLL in the motor drive system is the flux, so dc bias can be effectively suppressed by using a closed-loop flux observer [25].

In general, both the classical speed integration scheme and the PLL scheme can realize vector control. However, the former is easily affected by the change of T_{r}, while the latter has errors in the speed ramps, and is also affected by harmonics, dc bias, and parameter changes. Although many scholars have proposed effective solutions to the above problems, they increase the complexity of the algorithm and make it difficult to reproduce. In addition, due to the different degrees of meticulousness used by different schemes, the control performance and complexity will be different.

The IM drive strategy without angle detection can effectively avoid the increase in algorithm complexity caused by detection accuracy. Predictive torque control (PTC) is a classical control strategy for IM that does not require a flux angle. It can be implemented in the static coordinate system, but it introduces additional weighting factor tuning problems [1].

Motivated by the above analysis, in this work we propose a predictive power control strategy with a simplified control structure for IM drives. Main contributions are as follows.

1) The instantaneous power theory is utilized here to simplify the control structure, which needs no rotor flux angle information, and eliminate complex position observer design.
2) A rotor flux observer with enhanced stability in the stationary coordinate system is proposed, which achieves a wide stable operation range.

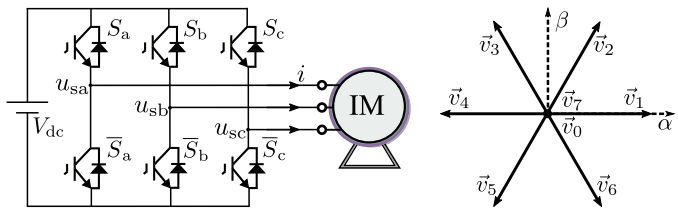

Fig. 1. Left: The topology of two-level voltage source converter with induction motor. Right: Fundamental voltage vectors.

3) Compared with classical predictive control strategies under the same working conditions, the proposal shows better control performances and simplified control realization.

The rest of this article is organized as follows. Section II introduces the mathematical model of the system used in the paper. In Section III, the classical predictive control strategies of IM drives are introduced. Section IV is the proposed predictive power control. In Section V, the proposed method is verified by hardware-in-the-loop (HiL) and experimental results. Finally, Section VI concludes this article.

II. System Model

The topology studied in this article is a two-level voltage source converter (VSC) with IM, which is shown in Fig. 1. Since the proposed method does not detect rotor flux angle, the system modeling will be completed in the stationary coordinate system. The model of power converter and IM will be introduced in this section, respectively.

A. Converter Model

The topology of a three-phase VSC with IM is shown in Fig. 1. S_{a}, S_{b}, and S_{c} represent the switching states of the three-phase. $S_{\mathrm{x}}=1$ represents that the upper bridge arm is ON and the lower bridge arm is OFF. $S_{\mathrm{x}}=0$ represents that the upper bridge arm is OFF and the lower bridge arm is ON ($x\in\{\mathrm{a},\mathrm{b},\mathrm{c}\}$). Therefore, the output voltage of the three-phase VSC can be expressed as follows:

$$\boldsymbol{u_{\mathrm{s}}}=\frac{2}{3}V_{\mathrm{dc}}(S_{\mathrm{a}}+\boldsymbol{a}S_{\mathrm{b}}+\boldsymbol{a}^2S_{\mathrm{c}}) \tag{1}$$

where $\boldsymbol{a}=e^{\mathrm{j}\frac{2\pi}{3}}$, V_{dc} is the dc link voltage of VSC. They can form eight fundamental voltage vectors, as shown in Fig. 1.

B. Motor Model

The squirrel cage IM is modeled in this part. Its fundamental equations can be expressed as

$$\boldsymbol{u_{\mathrm{s}}}=R_{\mathrm{s}}\boldsymbol{i_{\mathrm{s}}}+\frac{d\boldsymbol{\psi_{\mathrm{s}}}}{dt} \tag{2a}$$

$$\boldsymbol{\psi_{\mathrm{s}}}=L_{\mathrm{s}}\boldsymbol{i_{\mathrm{s}}}+L_{\mathrm{m}}\boldsymbol{i_{\mathrm{r}}} \tag{2b}$$

$$0=R_{\mathrm{r}}\boldsymbol{i_{\mathrm{r}}}+\frac{d\boldsymbol{\psi_{\mathrm{r}}}}{dt}-j\omega\boldsymbol{\psi_{\mathrm{r}}} \tag{2c}$$

$$\boldsymbol{\psi_{\mathrm{r}}}=L_{\mathrm{m}}\boldsymbol{i_{\mathrm{s}}}+L_{\mathrm{r}}\boldsymbol{i_{\mathrm{r}}} \tag{2d}$$

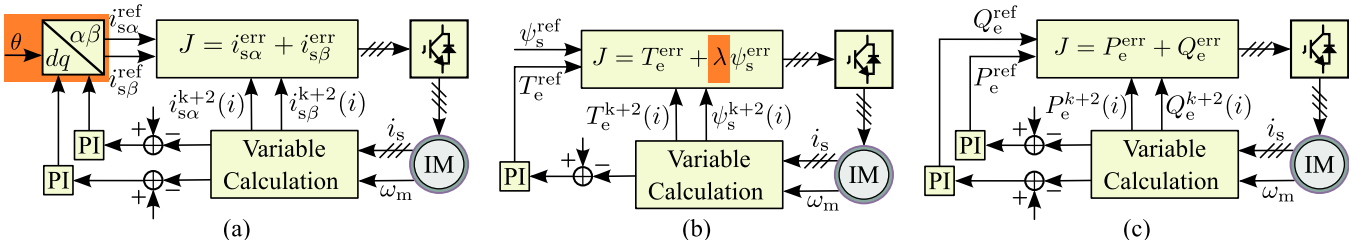

Fig. 2. Simplified control diagram of (a) PCC, (b) PTC, and (c) proposed PPC. The proposed strategy eliminates the phase detection and weighting factor, which are highlighted in (a) and (b).

where $\boldsymbol{i_s}$ and $\boldsymbol{\psi_s}$ are the stator current and flux, respectively. $\boldsymbol{i_r}$ and $\boldsymbol{\psi_r}$ are the rotor current and flux. R_s and L_s are the stator resistance and inductance, respectively. R_r and L_r are the rotor resistance and inductance. L_m is the mutual inductance. ω is the electrical angular speed of rotor.

The stator and rotor flux interaction can generate electromagnetic torque and drive the motor to rotate. The corresponding equations can be expressed as

$$T_e = \frac{3}{2} N_p \boldsymbol{\psi_s} \times \boldsymbol{i_s} \tag{3}$$

$$J\frac{d\omega_m}{dt} = T_e - T_L - B(\omega_m) \tag{4}$$

where T_e and T_L are the electromagnetic and load torque, respectively. N_p is the number of pole-pairs. ω_m is the mechanical angular speed of rotor. $B(\omega_m)$ represents the friction torque related to the speed of the rotor.

III. Classical Predictive Control Strategies of Induction Motor Drives

The nature of finite control set MPC is the optimization of cost function under the finite voltage vectors. The final result is to output the selected switching vector that makes the cost function optimal. The cost function can be flexibly configured to control multiple objectives [26]. According to the different control objectives, there are two classic predictive control strategies of IM drives, i.e., PCC and PTC, which will be described in this section. Their simplified control diagrams are shown in Fig. 2(a) and (b).

A. Predictive Current Control

The cost function of PCC can be expressed as

$$J = i_{s\alpha}^{err} + i_{s\beta}^{err} \tag{5}$$

where $i_{s\alpha}^{err} = [i_{s\alpha}^{ref} - i_{s\alpha}^{k+2}(i)]^2$, $i_{s\beta}^{err} = [i_{s\beta}^{ref} - i_{s\beta}^{k+2}(i)]^2$. $i = 0,...,7$, and it is determined by the converter used in the article. Because in the implementation of the algorithm, the time of calculation, measurements, and actuation is considerable. If the delay is not considered in the controller, the control performance will deteriorate. The delay compensation strategy is an effective way to solve this problem, i.e., $i_{s\alpha}^{k+2}(i)$ and $i_{s\beta}^{k+2}(i)$ are used in the cost function instead of $i_{s\alpha}^{k+1}(i)$ and $i_{s\beta}^{k+1}(i)$ [27]. This is why the predicted values in $k+2$ are used in (12), (23), and (24).

$i_{s\alpha}^{k+2}$ and $i_{s\beta}^{k+2}$ are the predictive value of stator current, which can be obtained from (2). Its predictive equation can be expressed as

$$\boldsymbol{i}_s^{k+1}(i) = \left(1 - \frac{T_s}{\tau_\sigma}\right)\boldsymbol{i}_s^k + \frac{T_s}{\tau_\sigma R_\sigma}\left[k_r\left(\frac{1}{\tau_r} - j\omega^k\right)\boldsymbol{\psi}_r^k + \boldsymbol{u}_s^k(i)\right] \tag{6}$$

where T_s is sampling time. $R_\sigma = R_s + k_r^2$, $\sigma = 1 - \frac{L_m^2}{L_s L_r}$, $k_r = \frac{L_m}{L_r}$, and $\tau_\sigma = \frac{\sigma L_s}{R_\sigma}$. $i_{s\alpha}^{ref}$ and $i_{s\beta}^{ref}$ are the reference value of stator current. Their equations can be expressed as

$$\begin{pmatrix} i_{s\alpha}^{ref} \\ i_{s\beta}^{ref} \end{pmatrix} = \begin{bmatrix} \cos(\theta) & \sin(\theta) \\ -\sin(\theta) & \cos(\theta) \end{bmatrix} \begin{pmatrix} i_{sd}^{ref} \\ i_{sq}^{ref} \end{pmatrix} \tag{7}$$

where i_{sd}^{ref} and i_{sq}^{ref} are the output of outer loop controller. θ is the angle of rotor flux. There are two classical methods to get it. The first is the speed integral, and the equation is

$$\theta = \int(\omega + \omega_s)dt \tag{8}$$

where $\omega_s = \frac{1}{T_r}\frac{L_m i_{sq}}{\psi_{rd}}$ is the slip speed of the motor. The performances of this method will be affected by the changes of R_r, because the rotor time constant T_r contains the rotor resistance R_r which varies with the working conditions of the motor. In addition, there is pure integral in the above method, which will also affect the control performances.

The second is through the PLL, whose transfer function is

$$G_{PLL} = \frac{\hat{\theta}_e}{\theta_e} = \frac{K_p s + K_i}{s^2 + K_p s + K_i} \tag{9}$$

where K_p and K_i are the control parameters of the loop filter in the PLL. According to the transfer function, the classical PLL is a second-order system, and there will be deviation at the speed ramps. Its existing improvement schemes and drawbacks have been introduced in the introduction. Besides, additional control parameters are introduced, which increases the effort of parameters tuning.

B. Predictive Torque Control

To obtain the predictive value of electromagnetic torque, it is necessary to predict the stator flux. The prediction equation can be expressed as

$$\boldsymbol{\psi}_s^{k+1}(i) = \boldsymbol{\psi}_s^k + T_s \boldsymbol{v}_s^k(i) - T_s \boldsymbol{i}_s^k R_s. \tag{10}$$

Based on the prediction equations of stator current and flux, the prediction equation of electromagnetic torque is

$$T_{\mathrm{e}}^{\mathrm{k+1}}(i)=\frac{3}{2}N_{\mathrm{p}}\boldsymbol{\psi}_{\mathrm{s}}^{\mathrm{k+1}}(i)\times\boldsymbol{i}_{\mathrm{s}}^{\mathrm{k+1}}(i). \tag{11}$$

The cost function of PTC can be expressed as

$$J=T_{\mathrm{e}}^{\mathrm{err}}+\lambda\psi_{\mathrm{s}}^{\mathrm{err}} \tag{12}$$

where $T_{\mathrm{e}}^{\mathrm{err}}=[T_{\mathrm{e}}^{\mathrm{ref}}-T_{\mathrm{e}}^{\mathrm{k+2}}(i)]^2$, $\psi_{\mathrm{s}}^{\mathrm{err}}=[\psi_{\mathrm{s}}^{\mathrm{ref}}-\psi_{\mathrm{s}}^{\mathrm{k+2}}(i)]^2$. λ is the weighting factor. $T_{\mathrm{e}}^{\mathrm{ref}}$ and $\psi_{\mathrm{s}}^{\mathrm{ref}}$ are the reference of torque and stator flux, respectively. Because the physical dimensions of torque and flux are different, it is necessary to add a weighting factor to the cost function. However, finding the appropriate weighting factor is still a problem [1].

IV. Proposed Predictive Power Control of Induction Motor Drives

Aiming at the flux angle detection and weighting factor elimination in classical PCC and PTC, the predictive power control (PPC) with simplified control architecture is proposed and the detail will be introduced in this section. The corresponding relationship between instantaneous active power and electromagnetic torque, instantaneous reactive power and rotor flux is analyzed, respectively. Based on this, the realization scheme of PPC is designed. In addition, the rotor flux observer in the stationary coordinate system may be unstable when the control frequency is low by analyzing its Lyapunov condition. Therefore, a more stable rotor flux observer is proposed as well.

A. Predictive Power Control

Based on the instantaneous power theory, the instantaneous active and reactive power of IM can be expressed as

$$P=u_{\mathrm{s}\alpha}i_{\mathrm{s}\alpha}+u_{\mathrm{s}\beta}i_{\mathrm{s}\beta}, \tag{13}$$

$$Q=u_{\mathrm{s}\beta}i_{\mathrm{s}\alpha}-u_{\mathrm{s}\alpha}i_{\mathrm{s}\beta}. \tag{14}$$

Based on (2), the instantaneous active power equation of IM can be rewritten as

$$\begin{aligned}P=&R_{\mathrm{s}}(i_{\mathrm{s}\alpha}^2+i_{\mathrm{s}\beta}^2)+\omega_{\mathrm{s}}k_{\mathrm{r}}(\psi_{\mathrm{r}\beta}i_{\mathrm{s}\alpha}-\psi_{\mathrm{r}\alpha}i_{\mathrm{s}\beta})\\&+\omega k_{\mathrm{r}}(\psi_{\mathrm{r}\beta}i_{\mathrm{s}\alpha}-\psi_{\mathrm{r}\alpha}i_{\mathrm{s}\beta}).\end{aligned} \tag{15}$$

The first part is the instantaneous power consumed by the stator resistance, the second part is the instantaneous power consumed by the rotor resistance, and the third part is the electromagnetic power of the IM. Similarly, the instantaneous reactive power of IM can also be expressed as

$$\begin{aligned}Q=&-(\omega_{\mathrm{s}}+\omega)\sigma L_{\mathrm{s}}(i_{\mathrm{s}\alpha}^2+i_{\mathrm{s}\beta}^2)-\omega_{\mathrm{s}}k_{\mathrm{r}}\left(\psi_{\mathrm{r}\alpha}i_{\mathrm{s}\alpha}+\psi_{\mathrm{r}\beta}i_{\mathrm{s}\beta}\right)\\&+\omega k_{\mathrm{r}}(\psi_{\mathrm{r}\alpha}i_{\mathrm{s}\alpha}+\psi_{\mathrm{r}\beta}i_{\mathrm{s}\beta}).\end{aligned} \tag{16}$$

The third part is the excitation power corresponding to the electromagnetic power.

Next, the corresponding relationship between torque and electromagnetic power, rotor flux and excitation power will be analyzed. In the synchronous reference frame of rotor flux oriented, the excitation power can be expressed as

$$Q_{\mathrm{e}}=\omega k_{\mathrm{r}}\psi_{\mathrm{rd}}i_{\mathrm{sd}}. \tag{17}$$

Based on the relationship between rotor flux and stator current, the above equation can be expressed as

$$\psi_{\mathrm{rd}}^2=\frac{1}{T_{\mathrm{r}}s+1}\frac{Q_{\mathrm{e}}}{\omega k_{\mathrm{r}}}. \tag{18}$$

According to the above equation, the rotor flux can be controlled by the excitation power, in which the speed is controlled by the outer speed control loop. In the synchronous reference frame of the rotor flux oriented, the electromagnetic power can be expressed as

$$P_{\mathrm{e}}=\omega k_{\mathrm{r}}\psi_{\mathrm{rd}}i_{\mathrm{sq}}. \tag{19}$$

Based on the relationship between torque and electromagnetic power, the above equation can be expressed as

$$T_{\mathrm{e}}=\frac{P_{\mathrm{e}}}{\omega_{\mathrm{m}}}. \tag{20}$$

That is, the electromagnetic torque can be controlled by the electromagnetic power.

To realize the PPC of IM, it is necessary to find out the reference value of electromagnetic and excitation power. Based on the above analysis, the instantaneous power reference value can be expressed as

$$P_{\mathrm{e}}^{\mathrm{ref}}=T_{\mathrm{e}}^{\mathrm{ref}}\omega_{\mathrm{m}}^{\mathrm{ref}} \tag{21}$$

$$Q_{\mathrm{e}}^{\mathrm{ref}}=E_{\psi}^{\mathrm{ref}}\omega_{\mathrm{m}}^{\mathrm{ref}} \tag{22}$$

where $T_{\mathrm{e}}^{\mathrm{ref}}$ is the output of outer speed control loop that can not only realize the tracking of speed, but also generate part of the electromagnetic power reference value. E_{ψ}^{ref} is the output of the outer flux control loop. Its main function is to ensure that the two terms in the cost function have the same physical dimension and eliminate the weighting factor. $\omega_{\mathrm{m}}^{\mathrm{ref}}$ is the reference of speed which is the given value.

Therefore, the cost function of PPC can be expressed as

$$J=P_{\mathrm{e}}^{\mathrm{err}}+Q_{\mathrm{e}}^{\mathrm{err}} \tag{23}$$

where $P_{\mathrm{e}}^{\mathrm{err}}=[P_{\mathrm{e}}^{\mathrm{ref}}-P_{\mathrm{e}}^{\mathrm{k+2}}(i)]^2$ and $Q_{\mathrm{e}}^{\mathrm{err}}=[Q_{\mathrm{e}}^{\mathrm{ref}}-Q_{\mathrm{e}}^{\mathrm{k+2}}(i)]^2$. $P_{\mathrm{e}}^{\mathrm{k+2}}(i)$ and $Q_{\mathrm{e}}^{\mathrm{k+2}}(i)$ represent the predictive value of electromagnetic and excitation power, respectively. Considering the time of sampling and calculation, the time delay compensation is necessary [27].

Based on the predictive value of stator current and rotor flux, the predictive value of the electromagnetic and excitation power can be derived, which can be expressed as

$$P_{\mathrm{e}}^{\mathrm{k+2}}(i)=k_{\mathrm{r}}N_{\mathrm{p}}\omega_{\mathrm{m}}[\psi_{\mathrm{r}\alpha}^{\mathrm{k+2}}i_{\mathrm{s}\beta}^{\mathrm{k+2}}(i)-\psi_{\mathrm{r}\beta}^{\mathrm{k+2}}i_{\mathrm{s}\alpha}^{\mathrm{k+2}}(i)] \tag{24a}$$

$$Q_{\mathrm{e}}^{\mathrm{k+2}}(i)=k_{\mathrm{r}}N_{\mathrm{p}}\omega_{\mathrm{m}}[\psi_{\mathrm{r}\alpha}^{\mathrm{k+2}}i_{\mathrm{s}\alpha}^{\mathrm{k+2}}(i)+\psi_{\mathrm{r}\beta}^{\mathrm{k+2}}i_{\mathrm{s}\beta}^{\mathrm{k+2}}(i)]. \tag{24b}$$

To analyze the feasibility of the proposed strategy conveniently, the synchronous reference system is introduced in (17), (18), and (19). In fact, the synchronous reference system is not used when the strategy is implemented in the controller according to (23) and (24).

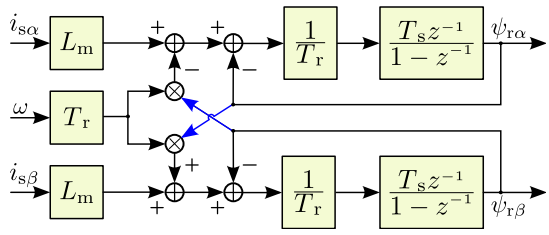

Fig. 3. Diagram of rotor flux observer based on the current model.

B. Rotor Flux Observer

In the classical rotor flux observer based on the voltage model, it is difficult to obtain stable rotor flux at low speed because of the small back electromotive force. It is an effective compensation method to add the rotor flux observer based on the current model. It does not need back electromotive force, avoiding the problem of a low signal-to-noise ratio at low speed. However, the flux observer based on the current model has cross-feedback in the stationary coordinate system, which may not converge in the digital controller. To eliminate the cross-feedback, the classical flux observer based on the current model is implemented in the synchronous reference frame, but the rotor flux angle needs to be introduced. In order to eliminate flux angle detection, a stable rotor flux observer is designed in the stationary coordinate system in this section, and its Lyapunov stability condition is analyzed.

The diagram of rotor flux observer based on the current model in the stationary coordinate system is shown in Fig. 3. Its state space expression can be expressed as

$$\psi_{\mathrm{ri}}^{\mathrm{k}+1} = \Phi\psi_{\mathrm{ri}}^{\mathrm{k}} + Hi_{\mathrm{s}}^{\mathrm{k}} \tag{25}$$

where $i_{\mathrm{s}} = [i_{\mathrm{s}\alpha}\ i_{\mathrm{s}\beta}]^{\mathrm{T}}$, $\psi_{\mathrm{ri}} = [\psi_{\mathrm{ri}\alpha}\ \psi_{\mathrm{ri}\beta}]^{\mathrm{T}}$

$$\Phi = \begin{bmatrix} 1-\frac{T_{\mathrm{s}}}{T_{\mathrm{r}}} & \omega T_{\mathrm{s}} \\ -\omega T_{\mathrm{s}} & 1-\frac{T_{\mathrm{s}}}{T_{\mathrm{r}}} \end{bmatrix}, \tag{26a}$$

$$H = \begin{bmatrix} \frac{T_{\mathrm{s}}L_{\mathrm{m}}}{T_{\mathrm{r}}} & 0 \\ 0 & \frac{T_{\mathrm{s}}L_{\mathrm{m}}}{T_{\mathrm{r}}} \end{bmatrix}. \tag{26b}$$

Based on the control theory of discrete systems, the condition that the flux observer satisfies Lyapunov stability is

$$T_{\mathrm{s}} \le \frac{2T_{\mathrm{r}}}{\omega^2 T_{\mathrm{r}}^2 + 1}. \tag{27}$$

In this experimental motor, as long as the control frequency is greater than 7.94 kHz, the observer satisfies the Lyapunov stability condition.

According to (27), the stability is related to the speed. The higher the ω, the higher the controller frequency required for system stability. To further reduce the requirement for control frequency, a stable flux observer is introduced. The current model is used at low speed, and the voltage model whose stability is independent of the control frequency, is selected at high speed. The scheme can be expressed as

$$\psi_{\mathrm{r}}^{\mathrm{k}+1} = F(z)\psi_{\mathrm{rv}}^{\mathrm{k}+1} + [1-F(z)]\psi_{\mathrm{ri}}^{\mathrm{k}+1} \tag{28}$$

TABLE I
SYSTEM PARAMETERS

Parameter	Symbol	Value
Sampling time	T_{s}	50 μs
DC-link voltage	V_{dc}	580 V
Stator inductance	L_{s}	113 mH
Rotor inductance	L_{r}	113 mH
Mutual inductance	L_{m}	107 mH
Stator resistance	R_{s}	0.688 Ω
Rotor resistance	R_{r}	0.262 Ω
Pair of poles	p	1
Rotational inertia	J	0.005kg/m^2

where $F(z)$ is the equation of the selection function [28]. In this article, $F(z) = \frac{1-z^{-1}}{1-z^{-1}+\omega_\psi T_{\mathrm{s}}}$ is used, and it can be adjusted according to the requirements. $\psi_{\mathrm{rv}}^{\mathrm{k}+1}$ is the predictive value of rotor flux based on the voltage model. The expression of the flux observer based on the voltage model in the stationary coordinate system can be expressed as

$$\psi_{\mathrm{rv}}^{\mathrm{k}+1} = \psi_{\mathrm{rv}}^{\mathrm{k}} + \frac{L_{\mathrm{r}}T_{\mathrm{s}}}{L_{\mathrm{m}}}\left(\boldsymbol{v}_{\mathrm{s}}^{\mathrm{k}} - \boldsymbol{i}_{\mathrm{s}}^{\mathrm{k}}R_{\mathrm{s}}\right) - \sigma L_{\mathrm{s}}\left(\boldsymbol{i}_{\mathrm{s}}^{\mathrm{k}+1} - \boldsymbol{i}_{\mathrm{s}}^{\mathrm{k}}\right). \tag{29}$$

In the implementation of the proposed scheme, the selected $F(z)$ cancels out the pure integration of the flux observer based on the voltage model, effectively avoiding the dc bias.

The simplified control diagram of the three aforementioned control techniques is shown in Fig. 2, and the simplified part is highlighted.

V. EFFECTIVENESS VERIFICATION

In this section, the transient and steady-state performance of the proposed PPC is compared with that of the PCC and PTC through experimental and HiL results. The influence of stator resistance R_{s} and mutual inductance L_{m} variation on the PCC and PPC is compared through experiments and HiL. In addition, to emphasize the contributions of the proposed PPC, the comparative experiments with the strategy proposed in [29] are completed.

Fig. 14 is the experimental hardware. The load torque is provided by a permanent magnet synchronous motor driven by a commercial converter. Measured speed and currents are used to drive the motor. The control frequency of the three predictive control strategies is 12.5 kHz. The system parameters of the tested IM are shown in Table I. The parameters of outer speed controller are as follows: $k_{\mathrm{p}\omega} = 0.66$ and $k_{\mathrm{i}\omega} = 4$. The parameters of outer flux controller are $k_{\mathrm{p}\psi} = 15$ and $k_{\mathrm{i}\psi} = 3$.

A. HiL Results

To verify the effectiveness of the proposed PPC, the transient and steady state performances of the PCC, PTC, and PPC are compared. To ensure comparison under the same operating conditions, the torque reference T_{e} for PTC is changed into the product of $\frac{3}{2}N_{\mathrm{p}}$, $\psi_{\mathrm{s}}^{\mathrm{ref}}$, and $i_{\mathrm{sq}}^{\mathrm{ref}}$, where $i_{\mathrm{sq}}^{\mathrm{ref}}$ is the output of the outer speed loop controller. The control parameters are

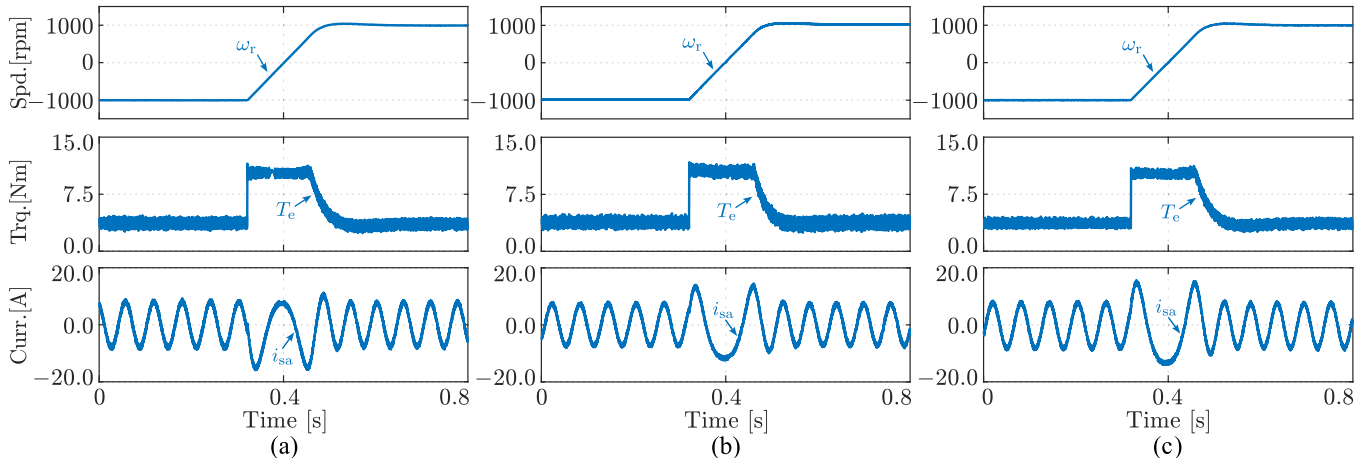

Fig. 4. HiL results of reversal from –1000 to 1000 r/min under the same conditions with the same equivalent outer-loop controller parameters. (a) PCC. (b) PTC. (c) Proposed PPC.

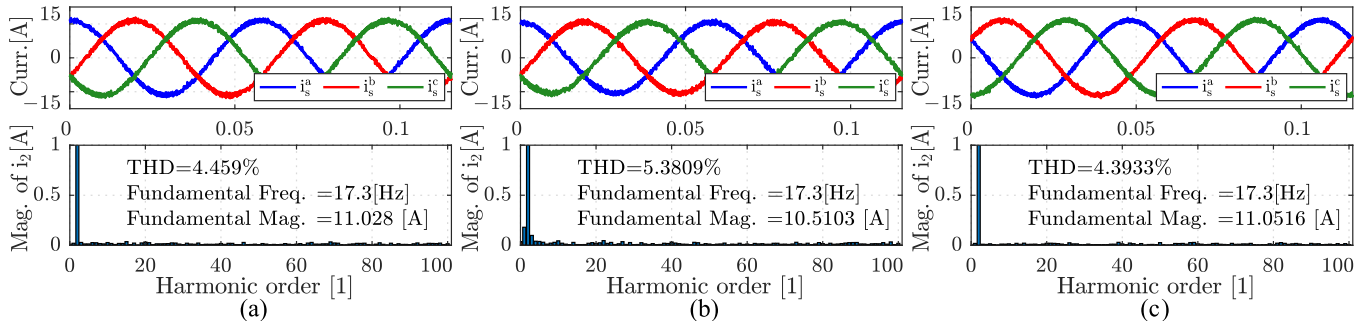

Fig. 5. HiL results of steady-state under the same conditions with the same equivalent outer-loop controller parameters. (a) PCC. (b) PTC. (c) Proposed PPC.

$k_{\mathrm{p}\omega}^{\mathrm{HiL}} = 0.3$ and $k_{\mathrm{i}\omega}^{\mathrm{HiL}} = 5$, which are consistent with PCC and PPC. To avoid the influence of the weighting factor on the control performance as far as possible, the weighting factor is adjusted so that the switching frequency of PTC is basically the same as PCC and PPC, fluctuating around 6.6 kHz. It can be seen from Figs. 4 and 5 that the performance of the three control strategies is similar under the same working conditions. However, through specific data analysis, the acceleration time from –1000 to 1000 r/min of PCC and PPC is longer (151 ms), while that of PTC is slightly faster (140 ms). This is related to electromagnetic torque in the acceleration stage. In the full acceleration phase, when the stator current limiting value is the same, the maximum average output torque of PCC and PTC is 11.7 Nm, while that of PTC is 12.3 Nm, which makes the dynamic response faster. However, according to the results of stator current analysis, the current control performance of PPC and PCC is better, with THD of 4.39% and 4.459%, respectively, while that of PTC is 5.38%, which is shown in Fig. 5. Based on the above analysis, the control effect of the three strategies is slightly different, and all of them can obtain good control performance. In addition, compared with PCC, the proposed strategy does not require rotor flux angle detection. Compared with PTC, the PPC does not need a weighting factor.

The steady-state performance of PCC and PPC with stator resistance R_{s} and mutual inductance L_{m} changes are completed, respectively. The performance of PTC does not shown here, because that of PTC and PCC has been compared in [30]. In light of the results in Fig. 6(a) and (b), the control performance when the observed R_{s} is 50%, 100%, and 200% of the actual value is verified, respectively. The torque variances of PCC under the three working conditions are 0.1016, 0.0885, and 0.0876, while those of PPC are 0.0772, 0.0827, and 0.0894. In general, both PCC and PPC can operate stably when R_{s} varies in the range of 0.5 to 1.5 times. To compare the effects of L_{m} changes, the results of PCC and PPC when the observed L_{m} is 0.95, 1, and 1.05 times of the actual value are shown in Fig. 6(c) and (d). The torque variances of PCC under the three working conditions are 0.4290, 0.1007, and 0.2366, while those of PPC are 0.4258, 0.0864, and 0.1721. In the process of L_{m} changes, the maximum speed drop of PCC is 47.7 r/min, while that of PPC is 44.8 r/min. In addition, as shown in Fig. 6(c) and (d), the torque and speed of PCC fluctuate significantly when the observed L_{m} is large, but PPC can maintain stability. PPC is more robust to the change of L_{m} than PCC based on the above verification, because PPC has a simplified control structure, avoiding the accumulation error of rotor flux angle detection.

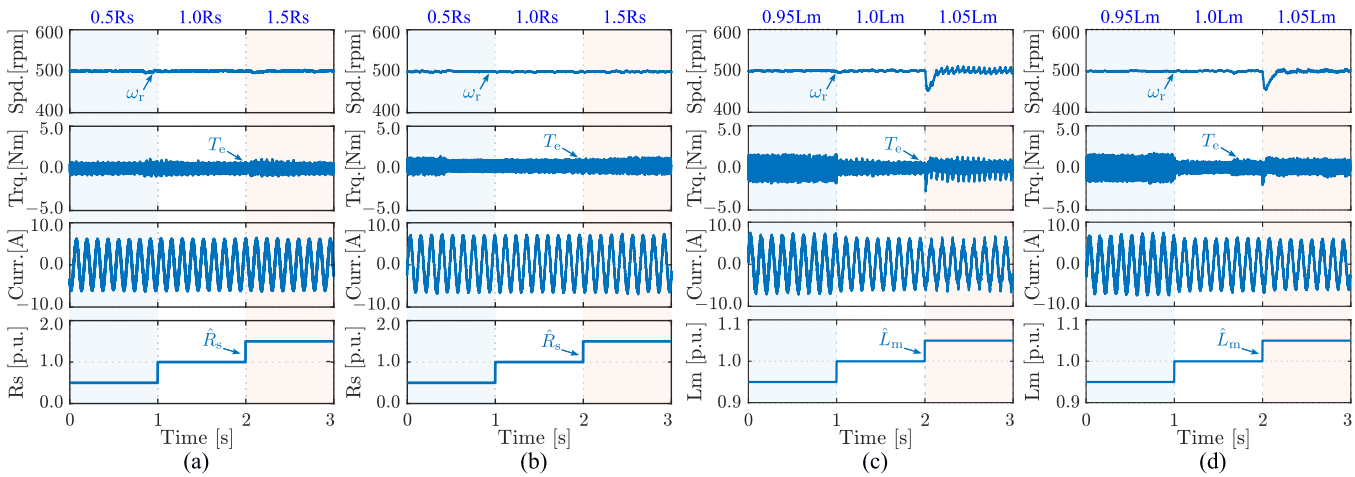

Fig. 6. HiL results of parameters variation under the same conditions. (a) and (b) are the R_s variation of PCC and the proposed PPC. (c) and (d) are the L_m variation of the PCC and the proposed PPC.

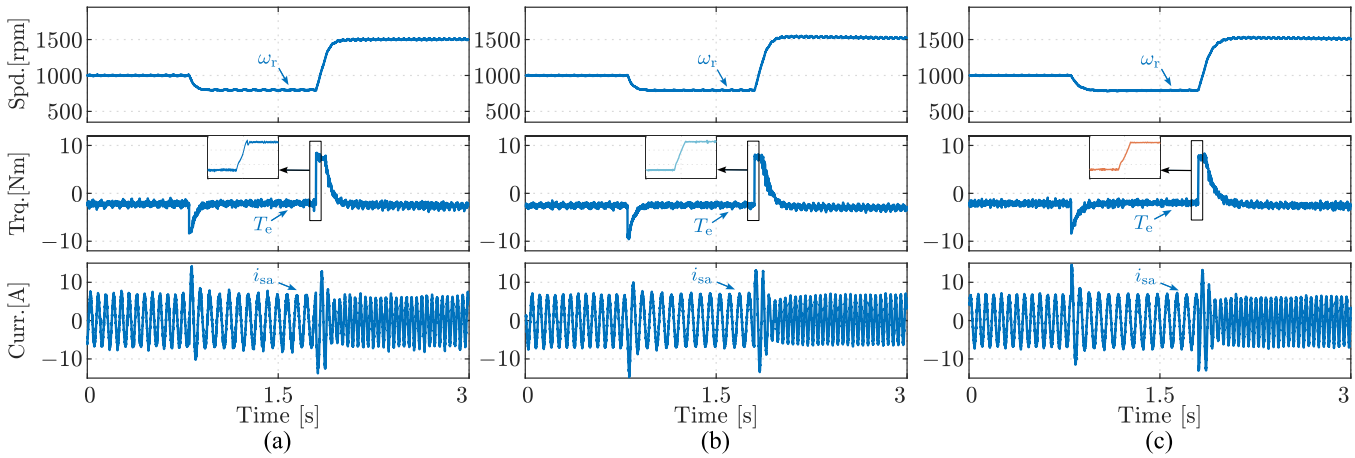

Fig. 7. Experimental results of decelerating from 1000 to 800 r/min and then accelerating to 1500 r/min under the same conditions with the same equivalent outer-loop controller parameters and weighting factor. (a) PCC. (b) PTC. (c) Proposed PPC.

B. Experimental Results

To further verify the effectiveness of the proposed strategy, the comparison experiments of PCC, PTC, and PPC are completed. The author first proposed PPC in [31], but the stability analysis and experimental verification were not given. In addition, the transient and steady state performance of the PPC and sequential predictive torque control (SPTC) proposed in [29] is compared by experiments under the same conditions.

Fig. 7 shows the experimental results of the PCC, PTC, and PPC during acceleration and deceleration. The deceleration time of the three strategies is 129 ms, 101 ms, and 102 ms, respectively, while the acceleration time is 199 ms, 165 ms, and 171 ms. Fig. 8 is the experimental results of the three control strategies during sudden load increase and decrease. To facilitate comparison, the actual data are shown in Fig. 8, and the torque is averaged every 1 ms, which is equivalent to filtering it. The speed and the averaged torque of the three strategies are placed in Fig. 9. According to the results, the speed and average torque curves of the three strategies basically coincide, which shows that their response to the load torque changes is similar. Based on the HiL results, all of PCC, PTC, and PPC can obtain great control performance. In the experimental results shown in Figs. 7, 8, and 9, the positive acceleration process with positive electromagnetic torque was retained, and the sudden load change and deceleration process with negative electromagnetic torque were added to verify more working conditions. In general, the experimental conclusion is consistent with that of HiL. The three strategies can track the reference value rapidly, but the maximum output torque of PTC is larger with the same stator current limiting. Therefore, its response speed is the fastest in the acceleration and deceleration stages, but the control effort of its stator current is the worst. PPC is more convenient to realize and easy to get good control performance with the simplified control structure.

Fig. 10 analyzes the influence of mutual inductance L_m changes on the proposed strategy through contrast experiments with PCC. As can be seen from the experimental results, both

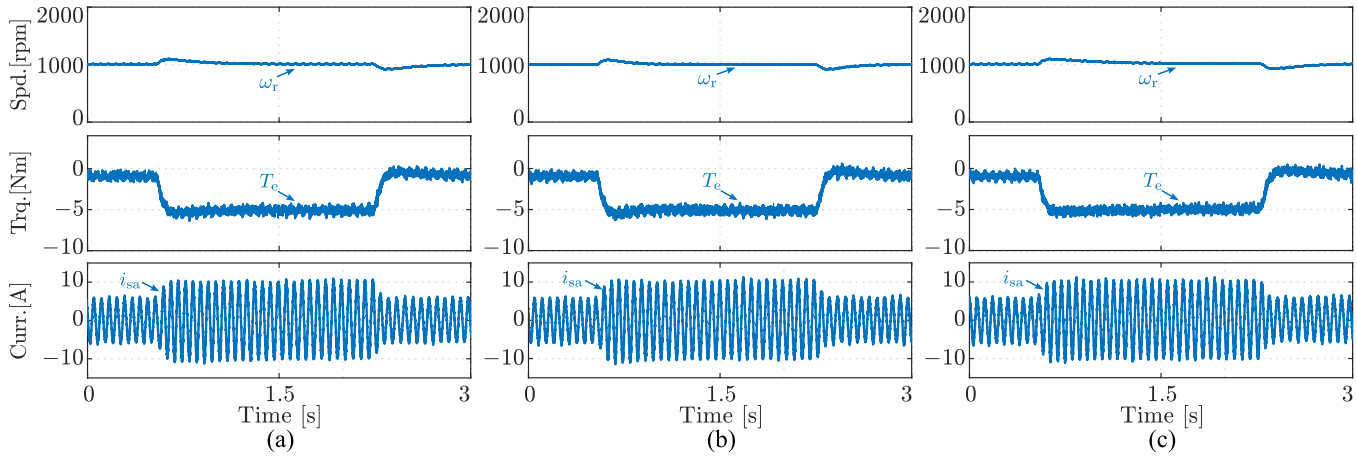

Fig. 8. Experimental results of transient-state during load abruptly change from –1 to –5 Nm and then to –1 Nm under the same conditions. (a) PCC. (b) PTC. (c) Proposed PPC.

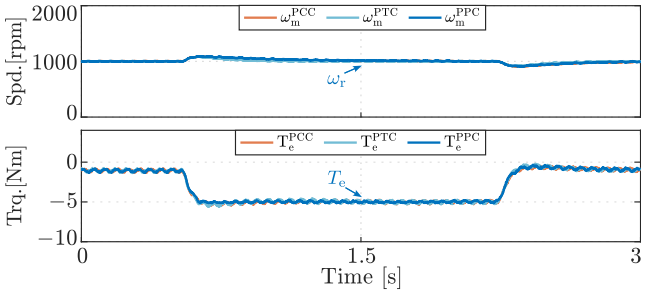

Fig. 9. Experimental results of PCC, PTC, and proposed PPC during load abruptly change: From top to bottom, this is speed and averaged torque.

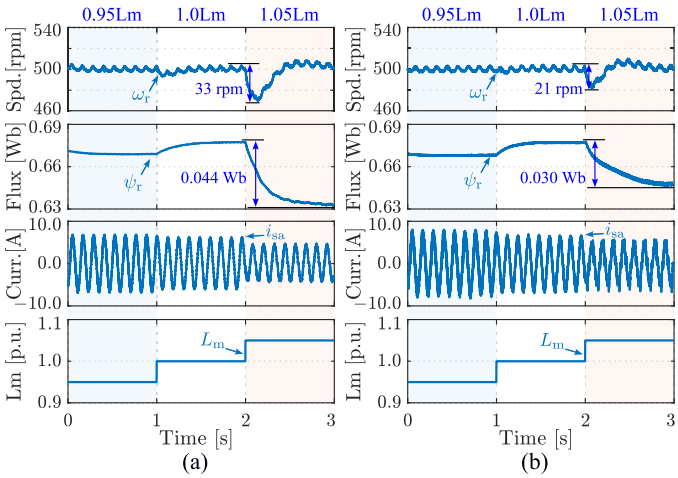

Fig. 10. Experimental results of the mutual inductance L_{m} variation under the same conditions. (a) PCC. (b) Proposed PPC.

strategies perform well when the observed value of L_{m} is smaller than the actual value. However, when the observed value is greater than the actual, the speed and rotor flux fluctuation of the proposed PPC is smaller than that of PCC. The speed drop of the PCC is 33 r/min, while that of the PPC is 21 r/min. The

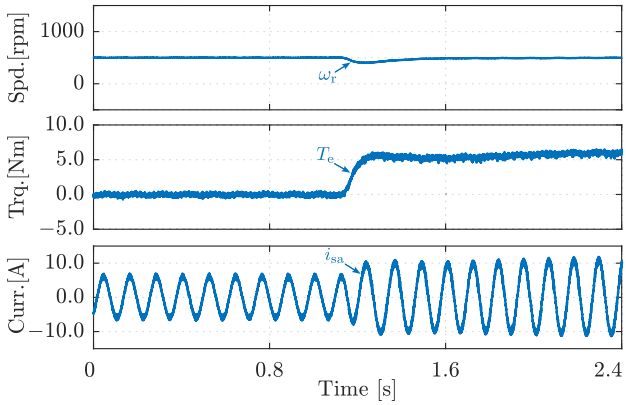

Fig. 11. Experimental results of SPTC during load abruptly increases from 0 to 5 Nm.

rotor flux of PCC drops by 0.044 Wb, while that of PPC is 0.03 Wb. According to the above results, the proposed PPC has better robustness to L_{m} changes, because the PPC simplifies the control structure and eliminates the angle detection that would accumulate errors.

Since the HiL cannot simulate all the details of the experiment, such as sampling noise and temperature changes, the results in Figs. 6 and 10 are not completely consistent. However, the conclusions of the comparison between PCC and PPC under the same conditions are consistent both in the experiment and HiL. Based on the HiL results shown in Fig. 6, the control performance of PPC is more robust to the change of L_{m} compared with PCC. This conclusion is further verified by the experimental results in Fig. 10.

According to the experimental results shown in Figs. 11 and 12, the transient response of the proposed strategy is faster when the load abruptly increases from 0 to 5 Nm, and the response time of the proposed PPC is 138 ms, while that of SPTC is 152 ms. Through the analysis of steady-state torque, the torque variance of SPTC is 0.0313, while that of PPC is 0.0417. By analyzing the steady-state stator currents, the THD of SPTC is

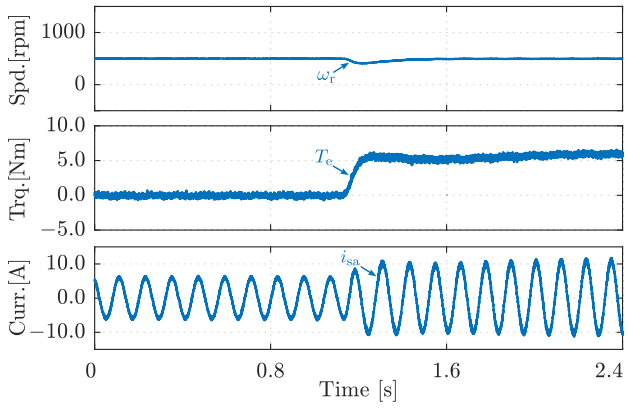

Fig. 12. Experimental results of proposed PPC during load abruptly increases from 0 to 5 Nm.

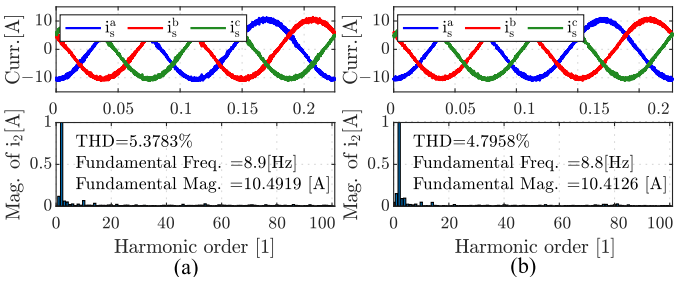

Fig. 13. Experimental results of steady-state under the same conditions. (a) SPTC. (b) Proposed PPC.

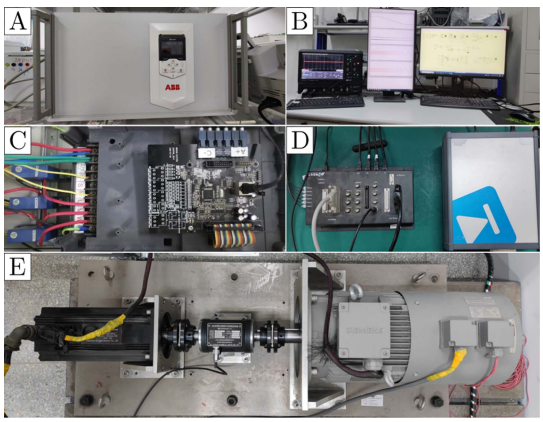

Fig. 14. Test bench setup for verifying the proposed methods. (a) Loading converter. (b) Upper computer. (c) Controlled converter. (d) Plexim RT-BOX real-time controller. (e) Load motor and drive motor.

5.39%, while that of PPC is 4.79%, which is shown in Fig. 13. According to the above results, both SPTC and PPC can achieve good control performance, but the transient response speed and steady-state stator current THD of the proposed PPC are better. This is because SPTC turns the weighting factor that can vary continuously in PTC into discrete weighting. The weighting of SPTC can be adjusted equivalently by changing the optimization order of the cost function and the number of selected vectors. The SPTC reduces the workload of weighting factor selection but also reduces the freedom to adjust the control performance. The proposed PPC can control the output active and reactive power with the same physical dimension without the weighting factor.

Based on the analysis of HiL and experimental results, PCC, PTC, and the proposed PPC can obtain good and similar control performance, although they are somewhat different in detail. Both PPC and SPTC can drive the IM without weighting factor and flux angle information, but the experimental comparison with SPTC shows that the control performance of the proposed strategy is better, because SPTC loses some optimization freedom due to the cascade structure. PCC also does not need the weighting factor, but its control performance could be affected by the accuracy of rotor flux angle detection, and the proposed PPC eliminates this link. Therefore, the control performance of the PPC is better than that of PCC when L_{m} changes. In general, the above results and analysis prove that the PPC can obtain good control effect with a simplified control architecture.

VI. Conclusion

To solve the problem that the control performance of the classical PCC heavily depends on the accuracy of rotor flux angle detection, this article proposes a PPC strategy. Compared with the PCC, the control framework of the proposed strategy is simplified, which does not require rotor flux angle detection. PTC also does not require rotor flux angle information, but it introduces cumbersome weighting factor selection. Compared with PTC, the proposed PPC does not require the weighting factor. In addition, a more stable flux observer in the stationary coordinate system is proposed, and the condition that the proposed method satisfies Lyapunov stability is analyzed. Experimental and HiL results show that the PPC can achieve sufficient control performance with the simplified control framework. When the parameters are accurate and consistent, the control performance of PPC is similar to that of PCC and PTC. Moreover, the proposed PPC is more robust to mutual inductance L_{m} variation than PCC.

Our future work will study more parameter-independent control strategies based on the proposed framework.

References

[1] J. Rodriguez et al., "Latest advances of model predictive control in electrical drives - Part II: Applications and benchmarking with classical control methods," *IEEE Trans. Power Electron.*, vol. 37, no. 5, pp. 5047–5061, May 2022.

[2] Q. Xing, Z. Zhang, Z. Li, X. Liu, Y. Li, and Y. Zhang, "Bias-free predictive control of power converters with LCL filter in micro-energy systems," *IEEE Trans. Ind. Electron.*, vol. 70, no. 6, pp. 5907–5916, Jun. 2023.

[3] B. Cavus and M. Aktas, "A new adaptive terminal sliding mode speed control in flux weakening region for DTC controlled induction motor drive," *IEEE Trans. Power Electron.*, vol. 39, no. 1, pp. 449–458, Jan. 2024.

[4] O. Babayomi and Z. Zhang, "Model-free predictive control of power converters with cascade-parallel extended state observers," *IEEE Trans. Ind. Electron.*, vol. 70, no. 10, pp. 10215–10226, Oct. 2023.

[5] P. Cao, X. Zhang, and S. Yang, "A unified-model-based analysis of MRAS for online rotor time constant estimation in an induction motor drive," *IEEE Trans. Ind. Electron.*, vol. 64, no. 6, pp. 4361–4371, Jun. 2017.

[6] K. Wang, W. Yao, B. Chen, G. Shen, K. Lee, and Z. Lu, "Magnetizing curve identification for induction motors at standstill without assumption of analytical curve functions," *IEEE Trans. Ind. Electron.*, vol. 62, no. 4, pp. 2144–2155, Apr. 2015.

[7] H. A. Toliyat, E. Levi, and M. Raina, "A review of RFO induction motor parameter estimation techniques," *IEEE Trans. Energy Convers.*, vol. 18, no. 2, pp. 271–283, Jun. 2003.
[8] S. A. Odhano, P. Pescetto, H. A. A. Awan, M. Hinkkanen, G. Pellegrino, and R. Bojoi, "Parameter identification and self-commissioning in AC motor drives: A technology status review," *IEEE Trans. Power Electron.*, vol. 34, no. 4, pp. 3603–3614, Apr. 2019.
[9] K. Wang, B. Chen, G. Shen, W. Yao, K. Lee, and Z. Lu, "Online updating of rotor time constant based on combined voltage and current mode flux observer for speed-sensorless AC drives," *IEEE Trans. Ind. Electron.*, vol. 61, no. 9, pp. 4583–4593, Sep. 2014.
[10] Z. Gao, T. G. Habetler, R. G. Harley, and R. S. Colby, "A sensorless rotor temperature estimator for induction machines based on current harmonic spectral estimation scheme," in *Proc. 12th Int. Power Electron. Motion Control Conf.*, 2006, pp. 431–437.
[11] Z. Masoumi, B. Moaveni, M. Khorshidi, J. Faiz, and S. M. M. Gazafrudi, "Experimental parameter estimation of induction motor based on transient and steady-state responses in synchronous and rotor reference frames," *IEEE Trans. Energy Convers.*, vol. 37, no. 1, pp. 145–152, Mar. 2022.
[12] S. M. Hasan and I. Husain, "A Luenberger-sliding mode observer for online parameter estimation and adaptation in high-performance induction motor drives," *IEEE Trans. Ind. Appl.*, vol. 45, no. 2, pp. 772–781, Mar./Apr. 2009.
[13] Y. Wang, N. Niimura, and R. D. Lorenz, "Real-time parameter identification and integration on deadbeat-direct torque and flux control (DB-DTFC) without inducing additional torque ripple," *IEEE Trans. Ind. Appl.*, vol. 52, no. 4, pp. 3104–3114, Jul./Aug. 2016.
[14] J. Zhang, X. Zhang, Y. Yu, B. Wang, and D. Xu, "A model reference adaptive system-based online rotor time constant estimation method for induction motor field-weakening control utilizing dot product of stator voltage and stator current," *IEEE Trans. Transport. Electrific.*, vol. 10, no. 2, pp. 3576–3589, Jun. 2024, doi: 10.1109/TTE.2023.3310517.
[15] X. Zhang, Y. Zhang, S. Yang, Z. Xie, and P. Cao, "An improved MRAS for rotor time constant updating in induction motor drives utilizing dot product of stator current and rotor flux," *IEEE Trans. Power Electron.*, vol. 34, no. 9, pp. 8905–8915, Sep. 2019.
[16] D. Chen, W. Kong, R. Qu, and L. Zhou, "Correction of field orientation inaccuracy caused by resolver periodic error and rotor time constant variation for indirect field-oriented control induction motor drives," *IEEE Trans. Ind. Electron.*, vol. 69, no. 5, pp. 4440–4450, May 2022.
[17] M. Wlas, Z. Krzeminski, and H. A. Toliyat, "Neural-network-based parameter estimations of induction motors," *IEEE Trans. Ind. Electron.*, vol. 55, no. 4, pp. 1783–1794, Apr. 2008.
[18] L. Zhao, J. Huang, J. Chen, and M. Ye, "A parallel speed and rotor time constant identification scheme for indirect field oriented induction motor drives," *IEEE Trans. Power Electron.*, vol. 31, no. 9, pp. 6494–6503, Sep. 2016.
[19] H. Wang, Y. Yang, X. Ge, Y. Zuo, Y. Yue, and S. Li, "PLL- and FLL-Based speed estimation schemes for speed-sensorless control of induction motor drives: Review and new attempts," *IEEE Trans. Power Electron.*, vol. 37, no. 3, pp. 3334–3356, Mar. 2022.
[20] M. K. Ghartemani, S. A. Khajehoddin, P. K. Jain, and A. Bakhshai, "Problems of startup and phase jumps in PLL systems," *IEEE Trans. Power Electron.*, vol. 27, no. 4, pp. 1830–1838, Apr. 2012.
[21] H. Wang, X. Ge, Y. Yue, and Y. C. Liu, "Dual phase-locked loop-based speed estimation scheme for sensorless vector control of linear induction motor drives," *IEEE Trans. Ind. Electron.*, vol. 67, no. 7, pp. 5900–5912, Jul. 2020.
[22] S. Golestan, J. M. Guerrero, and J. C. Vasquez, "Three-phase PLLs: A review of recent advances," *IEEE Trans. Power Electron.*, vol. 32, no. 3, pp. 1894–1907, Mar. 2017.
[23] S. Golestan, M. Ramezani, J. M. Guerrero, F. D. Freijedo, and M. Monfared, "Moving average filter based phase-locked loops: Performance analysis and design guidelines," *IEEE Trans. Power Electron.*, vol. 29, no. 6, pp. 2750–2763, Jun. 2014.
[24] H. Wang et al., "Speed-sensorless control of induction motor drives with a STA-FLL speed estimation scheme," *IEEE Trans. Ind. Electron.*, vol. 70, no. 12, pp. 12168–12180, Dec. 2023.
[25] P. Kanjiya, V. Khadkikar, and M. S. El Moursi, "Adaptive low-pass filter based DC offset removal technique for three-phase PLLs," *IEEE Trans. Ind. Electron.*, vol. 65, no. 11, pp. 9025–9029, Nov. 2018.
[26] B. Cavus and M. Aktas, "MPC-based flux weakening control for induction motor drive with DTC for electric vehicles," *IEEE Trans. Power Electron.*, vol. 38, no. 4, pp. 4430–4439, Apr. 2023.
[27] P. Cortes, J. Rodriguez, C. Silva, and A. Flores, "Delay compensation in model predictive current control of a three-phase inverter," *IEEE Trans. Ind. Electron.*, vol. 59, no. 2, pp. 1323–1325, Feb. 2012.
[28] Z. Zhang, Z. Li, M. P. Kazmierkowski, J. Rodriguez, and R. Kennel, "Robust predictive control of three-level NPC back-to-back power converter PMSG wind turbine systems with revised predictions," *IEEE Trans. Power Electron.*, vol. 33, no. 11, pp. 9588–9598, Nov. 2018.
[29] M. Norambuena, J. Rodriguez, Z. Zhang, F. Wang, C. Garcia, and R. Kennel, "A very simple strategy for high-quality performance of ac machines using model predictive control," *IEEE Trans. Power Electron.*, vol. 34, no. 1, pp. 794–800, Jan. 2019.
[30] F. Wang, S. Li, X. Mei, W. Xie, J. Rodríguez, and R. M. Kennel, "Model-based predictive direct control strategies for electrical drives: An experimental evaluation of PTC and PCC methods," *IEEE Trans. Ind. Informat.*, vol. 11, no. 3, pp. 671–681, Jun. 2015.
[31] J. Zhang et al., "Predictive power control of induction motor drives," in *Proc. IEEE 6th Int. Conf. Predictive Control Elect. Drives Power Electron.*, 2021, pp. 524–529.

Jin Zhang (Student Member, IEEE) was born in Shandong, China, in 1999. He received the B.S. degree in electrical engineering in 2021 from the School of Electrical and Power Engineering, Shandong University, Jinan, China, where he is currently working toward the master's degree in electrical engineering with the Lab of More Power Electronics Energy Systems, School of Electrical Engineering.

His research interests include power electronics and electrical drives, and advanced control of motor drives.

Zhenbin Zhang (Senior Member, IEEE) was born in Shandong, China, in 1984. He received the Ph.D. (*summa cum laude*) degree in electrical and energy engineering from the Technical University of Munich, Munich, Germany, in 2016.

He was a Postdoctoral in Electrical and Energy Engineering with the Technical University of Munich. Since 2017, he has been a Full Professor with Shandong University, Jinan, China, where he is currently the Director for both the Lab of More Power Electronics Energy Systems and the Institute of Sustainable Energy and Smart Grids. His research interests include power electronics and electrical drives, sustainable energy system, and smart and microgrids.

Dr. Zhang was the recipient for VDE Award-2017 in Suedbayern, Germany, and an Associate Editor for IEEE TRANSACTIONS ON POWER ELECTRONICS. He is currently an IET Fellow Member and IET Chartered Engineer.

Zhen Li (Member, IEEE) was born in Shandong, China, in 1983. She received the Ph.D. degree in power electronic semiconductor materials with Friedrich Alexander University Erlangen-Nurnberg (FAU), Erlangen, Germany, in 2017.

From 2014 to 2015, she was a Teaching and Research Assistant with FAU. From 2019, she has been an Associate Professor with Shandong University, Jinan, China. Her research interests include wide-band-gap devices and power converter reliability.

Haitao Li (Student Member, IEEE) was born in Shandong, China, in 1999. He received the B.Sc. degree in electrical engineering in 2021 from Shandong University, Jinan, China, where he is currently working toward the Ph.D. degree in electrical engineering with the Lab for More Power Electronic Energy Systems, School of Electrical Engineering.

His research interests include sensorless ac motor drives and offshore wind generation.

Yongdu Wang (Student Member, IEEE) was born in Shandong, China, in 1996. He received the B.S. and M.S. degrees in electrical engineering from the School of Electrical Engineering, Shandong University, Jinan, China, in 2018 and 2021, respectively. He is currently working toward the Ph.D. degree in electrical engineering with the Chair of High-Power Converter Systems, Technical University of Munich, Germany.

From 2021 to 2023, he has been an Associate Engineer with Yantai Power Supply Company, State Grid Shandong Power Supply Company, Shandong, China. His research interests include power electronics and electrical drives, and advanced control of motor drives.

Shichang Zhou (Student Member, IEEE) was born in Harbin, China. He received the B.S. degree in electrical engineering in 2022 from the School of Electrical Engineering, Shandong University, Jinan, China, where he is currently working toward the master's degree in electrical engineering with the Lab of More Power Electronics Energy Systems, School of Electrical Engineering.

His research interests include sensorless control of ac motor drives and advanced control of high-speed motors.

Teng Long (Member, IEEE) received the B.Eng. degree in electrical engineering from the Huazhong University of Science and Technology, Wuhan, China, and the first class B.Eng. (first class Hons.) degree in electrical engineering from the University of Birmingham, Birmingham, U.K., in 2009, and the Ph.D. degree in engineering from the University of Cambridge, Cambridge, U.K., in 2013.

Until 2016, he was a Power Electronics Engineer with General Electric Power Conversion, Rugby, U.K. He is currently a Full Professor with the University of Cambridge. His research interests include power electronics, electrical machines, and machine drives.

Dr. Long is a Chartered Engineer (CEng) registered with the Engineering Council, U.K.